Intramolecular Proton Transfer in Calixphyrin Derivatives

Jan Horníček,[†,‡] Hana Dvořáková,[‡] and Petr Bouř*[,†]

Institute of Organic Chemistry and Biochemistry, Academy of Sciences, 166 10 Prague, Czech Republic, and NMR Laboratory, Institute of Chemical Technology, 166 28 Prague, Czech Republic

Received: December 7, 2009; Revised Manuscript Received: February 1, 2010

Calix[4]phyrins are convenient models for porphyrin metabolism intermediates. They also attract attention as complexation agents in macromolecular chemistry. For the biological function and chemical properties, their flexibility plays an important role. In this study, we explore the inner hydrogen motion previously detected in some calix[4]phyrins as a slow chemical exchange in the NMR spectra (*J. Am. Chem. Soc.* **2004**, *126*, 13714). The potential energy surface of this motion is defined by two generalized coordinates and modeled at DFT levels. The transitional barriers thus obtained agree reasonably well with those calculated from dynamic ^{1}H NMR measurements. The transitions over both the sp^2 and sp^3 links are found to be possible. During the transfer, an intermediate is formed where the two hydrogen atoms are attached to the neighboring nitrogens. Surprisingly, the barriers channeling the sp^2 and sp^3 paths in significantly depend on the dispersion and other interactions between remote side chains. The results confirm the possibility of a fine-tuning of the calixphyrin core properties by distant substituents.

Introduction

Calix[4]phyrins are a new class of compounds that can generally be obtained by a reduction of the −CH═ porphyrine group.[1] For example, an unsubstituted porphyrin (a) leads to the calix[4]phyrins-(1.*1*.1.*1*) (b)[2]

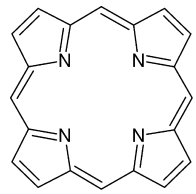

(a) Porphyrin

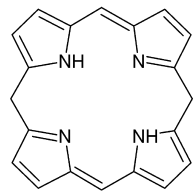

(b) Calixphyrin

The reduction makes the molecule more flexible, and calixphyrin derivatives are more prone to form complexes because the molecules can better adapt to ligands. The reduced porphyrin cycles also occur in many natural processes, such as porphyrin metabolic pathways including the heme synthesis. Their increased flexibility enhances the metabolism and enables a transfer across cellular membranes.[3,4]

The calixphyrins thus attracted attention as complexation agents[5−7] and components in macromolecular chemistry. Molecules based on calix[4]phyrins were proposed for electrochemical sensing.[8,9] Their chemical synthesis was elaborated so that relatively simple synthetic steps, such as the condensation of (perfluorophenyl)di(pyrrol-2-yl)methane with acetone,[10] could produce a large variety of substituted compounds.[1,5]

A closer analysis of calixphyrin NMR spectra revealed significant differences in flexibility of various derivatives.[10,11] The reduced porphyrin moiety can be almost planar, twisted, or bent; motion of covalently bound substituents is strongly dependent on the temperature. On the basis of density functional computations, several conformer species could be identified according to the observed changes in temperature-dependent ^{1}H NMR spectroscopy. In some compounds, the aryl group rotation and porphyrin ring flipping could be monitored independently as their NMR coalescence temperatures significantly differ.[11]

The compounds **p1**−**p3** (Figure 1) exhibited a low-temperature (∼−20−0 °C) ^{1}H NMR coalescence that was assigned to the motion of the inner acidic hydrogen atoms, but it could not be interpreted on the basis of a simple one-dimensional model.[10] Neither did the hydrogen motion simply correlate with the rate of other conformational toggling, nor could it be related to the substitutions of the sp^2 and sp^3 *meso*-carbon bridges. Because of the significance of the calixphyrin flexibility for their complexation and other chemical properties and also because of the relation of the intramolecular motion to the hydrogen-transfer processes encountered in photosynthesis and other biological energy cycles,[12] in the current study, we study the conformational motion in detail. Previous theoretical studies of the NH tautomerism in porphyrins suggest a tight relation of involved energies with the molecular structure.[13,14] The possibility of the inner hydrogen motion and an asynchronous mechanism was also suggested for porphyrazine.[15] For nonplanar porphyrins, an extraordinary propensity for intramolecular hydrogen binding was suggested.[16]

Although the motion of the two hydrogen atoms is a complex process, the multidimensionality can be reduced to 2 by a choice of suitable reaction path coordinates containing the difference of hydrogen−nitrogen distances. Optimization of molecular energies under restrictions on such generalized distance differences is not a part of available quantum chemical programs. Therefore, the restricted optimization has been performed by the Qgrad program using the vibrational normal-mode coordinates.[17] The program was recently extended by internal coordinate restrictions.[18] Thus, a two-dimensional potential energy surface (PES) corresponding to the hydrogen intermolecular transfer could be obtained at a relatively advanced DFT level

* To whom correspondence should be addressed. E-mail: bour@uochb.cas.cz.
† Academy of Sciences.
‡ Institute of Chemical Technology.

10.1021/jp911598w
Published on Web 02/16/2010

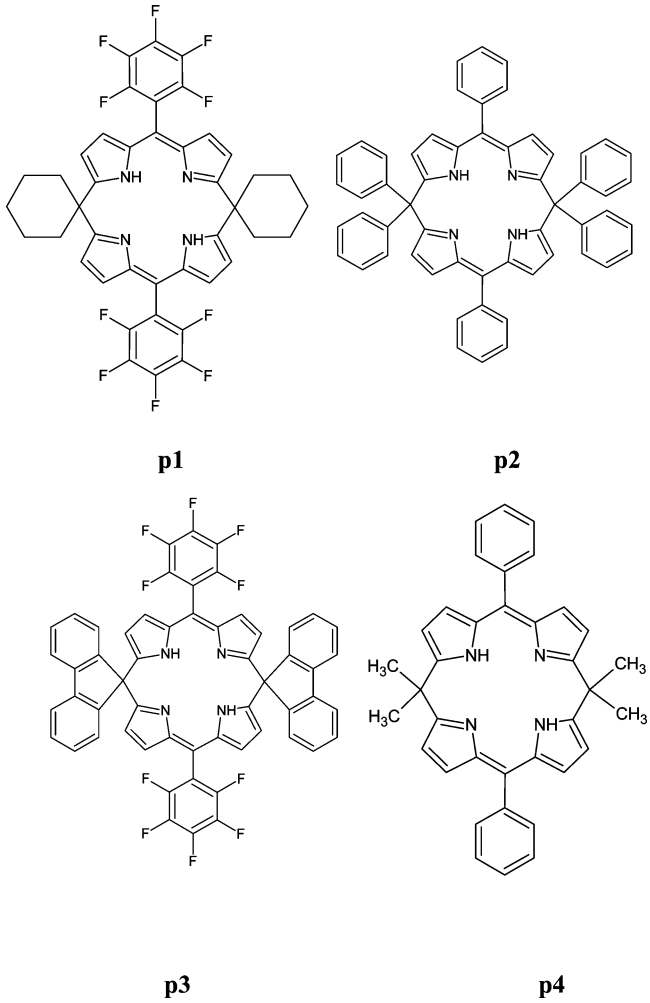

Figure 1. The four studied calix[4]phyrins.

of approximation. The proposed hydrogen-motion path over the sp^2 carbon could be verified and the barriers calculated from PES extremes compared to the experimental Gibbs energies.

Method

Experiment. The three studied compounds (**p1**, **p2**, and **p3**, Figure 1), where the transition temperatures of the hydrogen movement could be detected by NMR, were synthesized at the Institute of Chemical Technology, Prague. Complete experimental details about the chemical synthesis and NMR experiments can be found elsewhere.[10,11] The methylated compound (**p4**, Figure 1) was used as a computational model only and was not measured. The synthesis was based on a production of substituted dipyrromethanes, followed by condensation with aromatic aldehydes. The NMR spectra were measured on a Bruker DRX 500 Advance spectrometer operating at 500.1 MHz for ^{1}H and 125.8 MHz for ^{13}C. The compounds were measured in the temperature range of 193−298 K in CD_2Cl_2. Activation free energies (ΔG^*) were determined using the Eyring equations for the rate constant k[19]

$$k = \frac{k_B T_C}{h} e^{-\Delta G^*/RT_C} \quad (1)$$

$$k = \frac{\pi \Delta \nu}{\sqrt{2}} \quad (2)$$

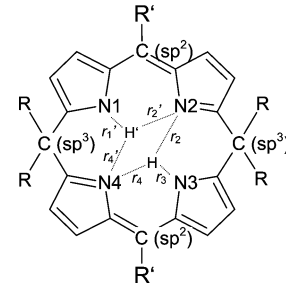

Figure 2. Definition of the distances (r_1', r_2', r_4', r_2, r_3, and r_4) describing positions of the two hydrogen atoms. Additional generalized coordinates for the simultaneous hydrogen transfer across the sp^2 link were used as $d = r_4 - r_3$ and $d' = r_2' - r_1'$. Similarly, for the sp^3 path, $d = r_2 - r_3$ and $d' = r_4' - r_1'$.

where, k_B is the Boltzmann constant, T_C the coalescence temperature, R the gas constant, h the Planck constant, and $\Delta\nu$ the chemical shift difference of the exchanging resonance in the absence of chemical exchange.

Computational Details. The positions of the inner hydrogen atoms were defined by their distances to the two nitrogen atoms between which the exchange NH···N ↔ N···HN takes place. For adiabatic potential energy scans, distance differences d and d' (cf. Figure 2) were used as generalized coordinates. The coordinates d and d' were kept constant at each of a 21 × 21 grid point, while all of the remaining coordinates were relaxed by energy minimization. The grid extended from −2 to 2 Å, with a 0.2 Å step. The Qgrad program[17,18] interfaced to Gaussian[20] was used for the adiabatic potential energy surface (PES) scan. The PM3,[21] HF/3-21G, and BPW91[22] levels of approximations were adopted. The BPW91 scan was performed for **p1** with the 6-31+G* basis functions for the two inner hydrogen atoms, 6-31G** functions for the reduced porphyrin ring, and the smallest 3-21G basis for the cyclohexane and perflourophenyl groups.

Alternatively, the transition barriers were calculated as energy differences between the equilibrium structure and transition geometries defined by $d = 0$ Å for one hydrogen. These calculations were performed at the B3LYP[23] and BPW91[22] levels with the 6-31G** basis set, using the Qgrad and Gaussian programs (which produced identical results); within the MP2 level, only single-point computations with DFT geometries could be done. For some DFT computations, the Grimme dispersion energy correction[24,25] was added as

$$E = -s_6 \sum_i \sum_{j>i} \frac{c_{ij}}{r_{ij}^6} f(r_{ij}) \quad (3)$$

where r_{ij} is the distance between atoms i and j, $f(r_{ij}) = (1 + \mathrm{ep})^{-1}$ is the damping function with $\mathrm{ep} = \exp(-D(r_{ij}/R_r - 1))$, s_6 is a global scaling factor, $D = 20$, R_r is a sum of atomic van der Waals (vdW) radii, and c_{ij} are the dispersion coefficients. The parameter values can be found in the original reference.[25] It is well known that the addition of the dispersion forces to common DFT functionals significantly enhances their performance, in particular, for systems with larger aromatic residues.[26]

Results and Discussion

Geometry. Selected geometry parameters of the **p1**−**p4** molecules are listed in Table 1. The experimental N−H distances for **p1**−**p3** are only approximate as the X-ray electronic densities do not allow for an accurate estimation of

TABLE 1: Selected Calculated and Experimental Geometry Parameters in the Calixphyrins p1−p4[a]

	PM3	HF/3-21G	BPW91/6-31G**	B3LYP/6-31G**	B3LYP/6-31G**[b]	exp.[c]
p1						
d(N−H)	1.01	1.00	1.03	1.02	1.02	0.87
d(N−N)/sp^2	2.64	2.75	2.74	2.75	2.74	2.73
d(N−N)/sp^3	3.11	3.00	3.07	3.05	3.02	3.02
τ	111	113	113	114	114	98
p2						
d(N−H)	0.99	1.00	1.03	1.02	1.02	0.86
d(N−N)/sp^2	2.97	2.88	2.84	2.83	2.77	2.79
d(N−N)/sp^3	2.93	2.91	2.96	2.95	2.95	2.92
τ	137	117	133	131	129	127
p3						
d(N−H)	0.99	1.00	1.02	1.01	1.01	0.90
d(N−N)/sp^2	2.84	2.93	3.01	2.94	2.86	2.89
d(N−N)/sp^3	3.03	2.90	2.86	2.90	2.92	2.91
τ	127	145	147	142	136	137
p4						
d(N−H)	1.01	1.00	1.03	1.02	1.02	
d(N−N)/sp^2	2.65	2.77	2.73	2.75	2.73	
d(N−N)/sp^3	3.10	2.99	3.07	3.05	3.02	
τ	119	122	120	121	120	

[a] Distances (d) are in Å; the τ angle between the two approximately planar moieties consisting of the sp^2-linked pyrrols is in degrees. [b] vdw-corrected. [c] Reference 10. Cambridge crystallographic database codes JAHHOQ (**p1**), JAHJAE (**p2**), and JAHHUW (**p3**).

hydrogen positions. The other experimental parameters, however, correlate with the computations quite well. They correctly reproduce the changes in the porphyrine core induced by the substituents. For example, the N−N distances across the sp^2 carbon bridge were calculated at the best vdw-B3LYP/6-31G** level as 2.74, 2.77, and 2.86 Å for **p1**, **p2**, and **p3**, respectively, which is in an excellent agreement with the X-ray data (2.73, 2.79, and 2.89 Å). The two pyrrol rings connected by the sp^2 bridge are approximately planar. However, the angle between these two planar moieties is very dependent on the substituents. Such dependence was observed for a larger set of compounds already in previous studies.[10,11] As discussed before,[11] the substituent influence is largely mediated by long-range electronic conjugation, which corresponds to the similarity of the geometry parameters in **p1** and **p4**, both with sp^3 substituents without π-electrons; the conformational restriction caused in **p1** by the cyclohexane ring does not appear so important.

The angle (τ in Table 1) in **p1** is calculated to be somewhat larger (∼114°) than the observed value (98°); we explain this by a tight crystal packing enabled by the relatively small cyclohexane ring. The crystal densities of **p1** (1.509 g/cm^3) and **p3** (1.513 g/cm^3) are similar and significantly differ from **p2** (1.227 g/cm^3). Additionally, in **p1**, the perflourophenyl residues are attracted to the NH groups of molecules in the next crystal layer, which keeps the angle τ small and stabilizes a $C_2/c15$ space symmetry group. In **p3**, the crystal packing is quite different, and the space group is *CC*9. The **p3** crystal additionally contains the chloroform solvent. Therefore, we suppose that the calculated **p1** structure is closer to that adopted in the chloroform solutions used for NMR than the crystal geometry.

Isomer Energies. On the adiabatic (relaxed) potential energy surface spanned by the positions of the two acidic hydrogen atoms, we calculated relative isomer energies of the extreme points summarized in Table 2. As expected from the behavior of common porphyrins,[14] in the lowest-energy global minimum structure (MG), the hydrogens occupy opposite nitrogen atoms ($r_1' = r_3$ or $r_2' = r_4$; see Figure 2). A jump of hydrogen across the sp^3 and sp^2 bridges leads to the M1 ($r_1' = r_4$) and M2 ($r_1' = r_2$) local minima, respectively, predicted to be energetically well-separated from the equilibrium structure. The relative energy of M2 is predicted to be 2−7 times smaller than that of M1. This can be explained by the hydrogen repulsion and a large space that can be occupied by these atoms in M2 due to their separation by the flexible sp^3 link. For both local minima, the energies are much larger than the Boltzmann quantum at the room temperature ($kT \sim 2.4$ kJ/mol), and corresponding populations are negligible under normal conditions.

TABLE 2: Relative Energies (kJ/mol) of Local Maxima and Minima for the p1−p4 Compounds

	p1	**p2**	**p3**	**p4**
MG (global min., $r_1' = r_3$; see Figure 2)	0	0	0	0
M1 (sp^3 local min., $r_1' = r_2$)				
HF/3-21G	127	99	98	112
B3LYP/6-31G**	91	73	64	86
B3LYP/6-31G**ΔG(273K)	86	64	63	77
M2 (sp^2 local min., $r_1' = r_4$)				
HF/3-21G	17	28	33	19
B3LYP/6-31G**	16	25	32	18
B3LYP/6-31G**ΔG(273K)	15	25	29	16
T1 (sp^3 saddle point, $r_1' = r_4'$)				
HF/3-21G	131	109	109	118
MP2/6-31G**[a]	22	149	10	18
B3LYP/6-31G**	90	74	69	84
B3LYP/6-31G**ΔG(273K)	77	59	64	69
vdw-B3LYP/6-31G/6-311++G**	58	121	54	56
T2 (sp^2 saddle point, $r_1' = r_2'$)				
PM3	81	101	104	91
HF/3-21G	75	92	110	71
MP2/6-31G**[a]	38	51	77	36
BPW91/6-31G**	31	45	61	28
BPW91/gen	29	46	57	28
B3LYP/6-31G**	44	58	74	42
B3LYP/6-31G**ΔG(273K)	35	53	67	30
vdw- B3LYP/6-31G**	43	54	69	41
vdw-B3LYP/6-31G/6-311++G**	47	60	81	43
experiment[10]	45	37	54	

[a] The vdw-B3LYP/6-31G/6-311++G** geometry.

For computational convenience, the saddle points (transition states) are defined for $r_1' = r_4'$ (T1) and $r_1' = r_2'$ (T2). These

structures slightly differ from the true saddle points because of the symmetry perturbation during the hydrogen migration; however, the deviation is quite minor (see below), and the error of the energies does not exceed ~1 kJ/mol. Therefore, we keep this definition as it enabled us to calculate the transition energies efficiently using internal molecular coordinates. Alternate QSTN[27] algorithms for localization of the transition states were not numerically stable enough to converge in a reasonable time. We can see that the T2 saddle point corresponding to the hydrogen path across the sp^3 linkage is energetically slightly preferred (by ~5−16 kJ/mol), most probably because of the stabilization of the bifurcated H−N bond in the vicinity of the transition state stabilized by the approximately planar dipyrrole unit and the π-electron conjugation. For **p3**, however, the sp^2 and sp^3 paths seem to be about equally probable as a planarity of the sp^3 link is partially enforced by the rigid fluorenyl substituent. From the Gibbs free energies (ΔG) calculated in Table 2 on the basis of vibrational harmonic functions, we can estimate that the entropic contribution is significant but does not change the qualitative differences between the individual compounds.

Although the size of the system does not allow for larger basis sets or benchmark wave function methods (the single-point MP2 computation lasted days at one processor (~3 GHz)), all of the investigated methods gave similar values of the T2 transition-state energies. It is interesting, that the van der Waals dispersion correction[24−26,28,29] also influenced the transition barrier, although the effect was restricted to ~1−5 kJ/mol (for the B3LYP/6-31G** level). The tension caused by the attraction of the distant hydrophobic residues was thus transferred to the conformational energetic of the acidic molecular core.

The T2 transition-state energies also correspond well to the experimental values[10] listed at the bottom of Table 2. The computed values for **p2** (e.g., 54 kJ/mol at the vdw-B3LYP/6-31G** level) deviate most from the experiment (37 kJ/mol); however, we find such accuracy acceptable because of the simplification used in the two-state transition model and ab initio modeling. The accuracy is also comparable with the predictions of other calixphyrin motions studied previously.[11] The presented computations thus also complete the explanations of the NMR coalescent events observed for the novel group of the calixphyrin compounds. Similarly as for the geometrical parameters, the relative energies in **p1** and **p4** are very close, which suggests a large role of the electron conjugation.[11]

Potential Energy Surface. The complete 2D adiabatic potential energy surface corresponding to the hydrogen sp^2 path in the d and d' coordinates (defined in Figure 2) calculated for **p1** at three different levels can be seen in Figure 3. The surfaces corresponding to the sp^3 path were similar and are not shown. The PM3, HF, and BPW91 methods provide qualitatively similar pictures; the PM3 method provides the highest barriers, while the BPW91 surface is the flattest. As can be seen, the T2 saddle point is very close to $d = 0$ (cf. Table 2), and this barrier thus determines the measured NMR transition rates. However, as the M1 minimum most probably lies on the reaction coordinate, the adopted two-state model may not be accurate, which can also explain some of the deviations between the measured and experimental numbers.

Figure 4 shows the differences in the calculated PESs for all three **p1**−**p3** compounds. Although the equilibrium geometries are rather similar, the energy profiles are notably different, which may explain the larger differences in the dynamical behavior of the calixphyrin compounds.[10] Finally, in Figure 5, we plot examples of the 2D vibrational wave function calculated in the

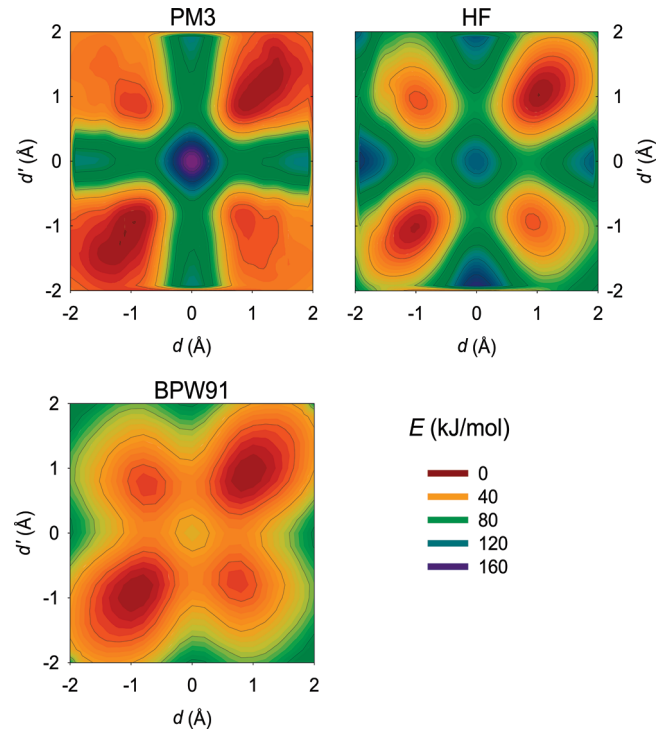

Figure 3. The two-dimensional potential energy surface corresponding to the hydrogen transfer in compound **p1**, calculated at the PM3, HF/3-21G, and BPW91/gen levels.

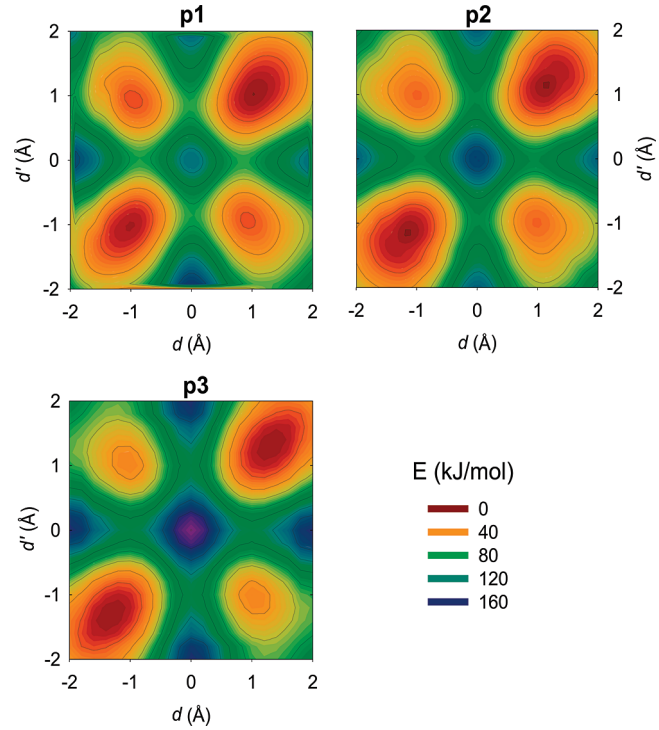

Figure 4. The calculated (HF/3-21G) potential energy surfaces for the **p1**, **p2**, and **p3** compounds.

generalized d and d' coordinates and the resultant probability distribution at 273 K. We can see that at equilibrium, the hydrogens are fairly localized. The izomerization observed by the dynamic NMR experiment thus corresponds to effectively simultaneous (on the NMR time scale) hydrogen transfer between well-defined binding sites. The intermediate states on the PES are weakly populated and cannot be detected; however,

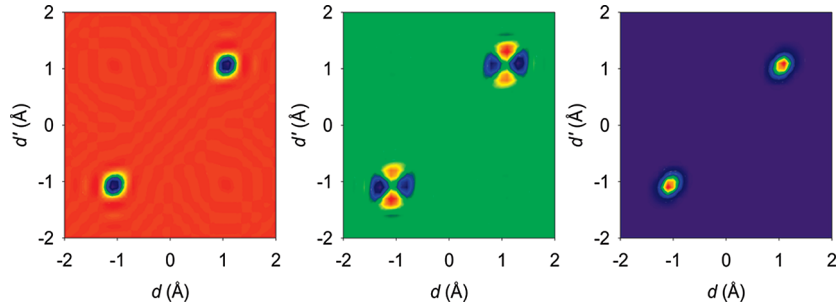

Figure 5. From left to right: Wave functions of the first and tenth vibrational state corresponding to the 2D hydrogen PES (HF/3-21G) and the probability distribution at 273 K.

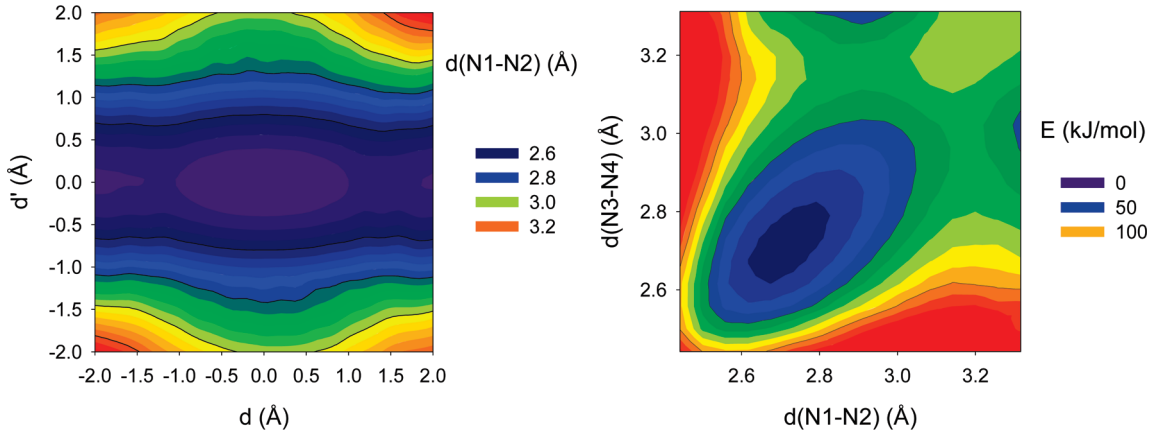

Figure 6. Calculated dependence (HF/3-21G) of the nitrogen distance on the hydrogen coordinate for the sp^2 path of **p1**.

a literally simultaneous event across the diagonal of the PES passing through the high-energy region is obviously not probable.

The hydrogen coordinates (Figure 2) were selected to drive the hydrogen movement. During molecular dynamics, the transfer can be actually caused by circumstances related to other coordinates, such as when the nitrogen atoms approach each other. In Figure 6 (left), the sp^2 N1−N2 distance in **p1** is plotted as a function of d and d'. Interestingly, the nitrogen atoms become close when the hydrogen is being transferred, which indicates a bifurcated bond. For a solitary transfer of one hydrogen, the remote nitrogen geometry is not significantly changed; however, as we saw above, the synchronous transfer is more probable. The energy profile recalculated for the d(N1−N2) and d(N3−N4) coordinates is plotted on the right-hand side of Figure 6. In the minimum, both distances adopt the equilibrium value (2.75 Å; see Table 1). The nitrogen distances are thus well-correlated with the hydrogen positions. For the static computations, however, the generalized hydrogen coordinates are more convenient as they provided the possibility to directly control the transfer.

Conclusions

On a series of three novel calixphyrin compounds, we investigated the energies associated with the hydrogen motion during an isomerization in the acidic molecular core. Experimental activation free energies (ΔG^*) obtained previously by ^{1}H NMR temperature-dependent measurements could be explained on the basis of a two-state transition model. The experimental free energies agreed well with the relative electronic energies obtained by quantum chemical computations. The largest deviation observed for the biphenyl derivative was attributed to a deviation from the two-state transition. The computations confirmed the possibility to tune the calixphyrin core properties by the distant substituents, which can be potentially used in preparation of complexation agents of desired behavior. The potential energy surfaces for the three compounds that could be determined by the introduction of the generalized coordinates were qualitative similar; the sp^2 hydrogen-transfer path seems to be favorable, except for the case when the fluorenyl substituent restricted the sp^3 link. The coupling of the quantum chemical methods with the NMR spectroscopy thus proved to be profitable, yielding new data about the molecular structure and dynamics.

Acknowledgment. The work was supported by the Grant Agency of the Czech Republic (Grants 203/06/0420, 202/07/0732) and Grant Agency of the Academy of Sciences (A400550702); access to the METACentrum computers (within the Project MSM6383917201) is also gratefully acknowledged.

References and Notes

(1) Král, V.; Sessler, J. L.; Zimmerman, R. S.; Seidel, D.; Lynch, V.; Andrioletti, B. *Angew. Chem., Int. Ed.* **2000**, *39*, 1055.

(2) Sessler, J. L.; Zimmerman, R. S.; Bucher, C.; Král, V.; Andrioletti, B. *Pure Appl. Chem.* **2001**, *73*, 1041.

(3) Karlson, P.; Gerok, W.; Gross, W. *Pathobiochemie*; Georg Thieme Verlag: Stuttgart, Germany, 1982.

(4) Battersby, A. R.; Fookies, C. J. R.; Matcham, G. W. J.; McDonald, E. *Nature* **1980**, *285*, 17.

(5) Bucher, C.; Devillers, C. H.; Moutet, J. C.; Royal, G.; Saint-Aman, E. *Coord. Chem. Rev.* **2009**, *253*, 21.

(6) Furuta, H.; Ishizuka, T.; Osuka, A. *Inorg. Chem. Commun.* **2003**, *6*, 398.

(7) Furuta, H.; Ishizuka, T.; Osuka, A.; Uwatoko, Y.; Ishikawa, Y. *Angew. Chem., Int. Ed.* **2001**, *40*, 2323.

(8) Bucher, C.; Devillers, C. H.; Moutet, J. C.; Pecaut, J.; Royal, G.; Saint-Aman, E.; Thomas, F. *Dalton Trans.* **2005**, 3620.

(9) Jha, S. C.; Lorch, M.; Lewis, R. A.; Archibald, S. J.; Boyle, R. W. *Org. Biomol. Chem.* **2007**, *5*, 1970.

(10) Dolenský, B.; Kroulík, J.; Král, V.; Sessler, J. L.; Dvořáková, H.; Bouř, P.; Bernátková, M.; Bucher, C.; Lynch, V. *J. Am. Chem. Soc.* **2004**, *126*, 13714.

(11) Bernátková, M.; Dvořáková, H.; Andrioletti, B.; Král, V.; Bouř, P. *J. Phys. Chem. A* **2005**, *109*, 5518.

(12) Karelson, M.; Pihlaja, K.; Tamm, T.; Uri, A.; Zerner, M. C. *J. Photochem. Photobiol., A* **1995**, *85*, 119.

(13) Kuzmitsky, V. A.; Solovyov, K. N. *J. Mol. Struct.* **1980**, *65*, 219.

(14) Wu, Y. D.; Chan, K. W. K.; Yip, C. P.; Vogel, E.; Plattner, D. A.; Houk, K. N. *J. Org. Chem.* **1997**, *62*, 9240.

(15) Huang, Y. Z.; Ma, S. Y. *J. Mol. Struct.: THEOCHEM* **2004**, *684*, 217.

(16) Somma, M. S.; Medforth, C. J.; Nelson, N. Y.; Olmstead, M. M.; Khoury, R. G.; Smith, K. M. *Chem. Commun.* **1999**, 1221.

(17) Bouř, P.; Keiderling, T. A. *J. Chem. Phys.* **2002**, *117*, 4126.

(18) Bouř, P. *Collect. Czech. Chem. Commun.* **2005**, *70*, 1315.

(19) Leskowitz, G. M.; Ghaderi, N.; Olsen, R. A.; Pederson, K.; Hatcher, M. E.; Mueller, L. J. *J. Phys. Chem. A* **2005**, *109*, 1152.

(20) Frisch, M. J.; Trucks, G. W.; Schlegel, H. B.; Scuseria, G. E.; Robb, M. A.; Cheeseman, J. R.; Montgomery, J. A., Jr.; Vreven, T.; Kudin, K. N.; Burant, J. C.; Millam, J. M.; Iyengar, S. S.; Tomasi, J.; Barone, V.; Mennucci, B.; Cossi, M.; Scalmani, G.; Rega, N.; Petersson, G. A.; Nakatsuji, H.; Hada, M.; Ehara, M.; Toyota, K.; Fukuda, R.; Hasegawa, J.; Ishida, M.; Nakajima, T.; Honda, Y.; Kitao, O.; Nakai, H.; Klene, M.; Li, X.; Knox, J. E.; Hratchian, H. P.; Cross, J. B.; Bakken, V.; Adamo, C.; Jaramillo, J.; Gomperts, R.; Stratmann, R. E.; Yazyev, O.; Austin, A. J.; Cammi, R.; Pomelli, C.; Ochterski, J. W.; Ayala, P. Y.; Morokuma, K.; Voth, G. A.; Salvador, P.; Dannenberg, J. J.; Zakrzewski, V. G.; Dapprich, S.; Daniels, A. D.; Strain, M. C.; Farkas, O.; Malick, D. K.; Rabuck, A. D.; Raghavachari, K.; Foresman, J. B.; Ortiz, J. V.; Cui, Q.; Baboul, A. G.; Clifford, S.; Cioslowski, J.; Stefanov, B. B.; Liu, G.; Liashenko, A.; Piskorz, P.; Komaromi, I.; Martin, R. L.; Fox, D. J.; Keith, T.; Al-Laham, M. A.; Peng, C. Y.; Nanayakkara, A.; Challacombe, M.; Gill, P. M. W.; Johnson, B.; Chen, W.; Wong, M. W.; Gonzalez, C.; Pople, J. A. *Gaussian 03*, revision C.02; Gaussian, Inc.: Wallingford, CT, 2004.

(21) Stewart, J. P. P. PM3. In *The Encyclopedia of Computational Chemistry*; Schleyer, P. v. R., Allinger, N. L., Clark, T., Gasteiger, J., Kollman, P. A., Schaefer, H. F., III, Schreiner, P. R., Eds.; John Wiley & Sons: Chichester, U.K., 1998; Vol. 2, p 2080.

(22) Becke, A. *Phys. Rev. A* **1988**, *38*, 3098.

(23) Becke, A. D. *J. Chem. Phys.* **1993**, *98*, 5648.

(24) Grimme, S. *J. Comput. Chem.* **2004**, *25*, 1463.

(25) Grimme, S. *J. Comput. Chem.* **2006**, *27*, 1787.

(26) Parchaňský, V.; Matějka, P.; Dolenský, B.; Havlík, M.; Bouř, P. *J. Mol. Struct.* **2009**, *934*, 117.

(27) Peng, C.; Ayala, P. Y.; Schlegel, H. B.; J., F. M. *J. Comput. Chem.* **1996**, *17*, 49.

(28) Schwabe, T.; Grimme, S. *Phys. Chem. Chem. Phys.* **2007**, *9*, 3397.

(29) Černý, J.; Hobza, P. *Phys. Chem. Chem. Phys.* **2005**, *7*, 1624.

JP911598W